




Beraprost sodium mitigates renal interstitial fibrosis through repairing renal microvessels

Shulin Li^{1,2} · Yanping Wang² · Lu Chen² · Zhuojun Wang² · Guodong Liu³ · Bangjie Zuo² · Caixia Liu² · Dong Sun^{1,2} 

Received: 28 September 2018 / Revised: 12 February 2019 / Accepted: 5 March 2019 / Published online: 28 March 2019
© Springer-Verlag GmbH Germany, part of Springer Nature 2019

Abstract

Beraprost sodium (BPS), as a prostacyclin analog, plays a significant role in various diseases based on its antiplatelet and vasodilation functions. However, its regulation and role in chronic kidney disease (CKD) still remain elusive. Here, we determined whether BPS could alleviate renal interstitial fibrosis, and improve the renal function and its therapeutic mechanism. In vitro, BPS increased angiogenesis in the HUVECs incubated with BPS detected by tube formation assay and repair damaged endothelial cell–cell junctions induced by hypoxia. In vivo, mice were randomly assigned to a sham-operation group (sham), a unilateral ureteral obstruction group (UUO), and a BPS intragastrical administration group (BPS), and sacrificed at days 3 and 7 post-surgery (six in each group). In UUO model, tissue hypoxia, renal inflammation, oxidative stress, and fibrotic lesions were detected by q-PCR and Western blot techniques and peritubular capillaries (PTCs) injury was detected by a novel technique of fluorescent microangiography (FMA) and analyzed by MATLAB software. Meanwhile, we identified cells undergoing endothelial cell-to-myofibroblast transition by the coexpression of endothelial cell (CD31) and myofibroblast (α-SMA) markers in the obstructed kidney. In contrast, BPS protected against interstitial fibrosis and substantially reduced the number of endothelial cell-to-myofibroblast transition cells. In conclusion, our data indicate the potent therapeutic of BPS in mitigating fibrosis through repairing renal microvessels and suppressing endothelial-mesenchymal transition (EndMT) progression after inhibiting inflammatory and oxidative stress effects.

Key messages

- BPS could improve renal recovery through anti-inflammatory and anti-oxidative pathways.
- BPS could mitigate fibrosis through repairing renal microvessels and suppressing endothelial-mesenchymal transition (EndMT).

Keywords Beraprost sodium · Peritubular capillaries · Inflammation · Oxidative stress · Endothelial-mesenchymal transition · Renal interstitial fibrosis

Shulin Li and Yanping Wang contributed equally to this work.

Electronic supplementary material The online version of this article (<https://doi.org/10.1007/s00109-019-01769-x>) contains supplementary material, which is available to authorized users.

✉ Caixia Liu
liucaixia2009@126.com

✉ Dong Sun
sundong126@yahoo.com

¹ Department of Internal Medicine and Diagnostics, Xuzhou Medical University, Xuzhou 221002, China

² Department of Nephrology, Affiliated Hospital of Xuzhou Medical University, 99 West Huai-hai Road, Xuzhou 221002, Jiangsu, China

³ Department of Orthopedics, The Second Affiliated Hospital of Xuzhou Medical University, Xuzhou 221006, China

Introduction

Chronic kidney disease (CKD) leading to end stage renal failure arises from many kidney damage. Renal fibrosis, characterized by oxidative stress, chronic inflammation, fibroblast proliferation and activation, extracellular matrix accumulation, and tubular atrophy, represents the final common outcome of a wide variety of progressive CKD [1, 2]. Several risk factors such as diabetes, hypertension, hyperuricemia, and smoking could be controlled by altering lifestyle or treating based on symptoms, but effective therapies that ameliorate the progression of CKD are still limited. Generating these effective therapies requires an understanding of the cellular and molecular mechanisms underlying CKD.

The kidney is a highly vascular organ, and the tubulointerstitium is particularly susceptible to injury, clinically resulting in the progress of CKD [3]. The renal peritubular capillaries delivering oxygen and nutrients to the tubules are crucial for the proper functioning of the kidney [4]. Several recent studies suggest capillary rarefaction and endothelial injury are important pathophysiological processes promoting renal fibrosis [5–7]. One explanation for this pathophysiology is tissue hypoxia. Such a hypoxic state of the kidney is primarily because of the decreased blood supply and increased oxygen demand and the augmented oxygen diffusion between arterial and venous vessels owing to the extracellular matrix accumulation [8, 9]. Loss of capillaries accompanied by hypoxia would induce an injury cascade with oxidative stress and inflammation [10]. Oxidative stress contributes significantly to progression of kidney disease by upregulating production of reactive oxygen species (ROS), which are critical players that can alter the structure and function of endothelial cells, and thereby induce EndMT and tubulointerstitial lesions [11]. Another central factor driving the pathogenesis of interstitial fibrosis is inflammation resulting from the production of pro-inflammatory molecules and leucocytic infiltration, which leading to subsequently more rapid loss of renal function [12, 13].

Prostaglandin I₂ (PGI₂), primarily synthesized in endothelial cells, has strong antiplatelet and vasodilation functions. As a prostacyclin analog, beraprost sodium (BPS) avoids prostacyclin's chemical instability and short plasma elimination half-life and becomes orally administered prodrug of PGI₂. Several studies have reported that BPS is a vasoactive substance, which has been used to treat pulmonary arterial hypertension [14], atherosclerosis obliterans [15], and microvascular complications of diabetic nephropathy [16] through expanding renal vessels, improving microcirculation. However, whether BPS could serve as a therapeutic tool to alleviate renal interstitial fibrosis has not been previously investigated. On the basis of previous studies, we hypothesized that BPS could alleviate renal interstitial fibrosis through improving renal microcirculation, further inhibiting inflammation and oxidative stress and ultimately suppressing EndMT. In this study, we sought to determine this hypothesis in both cells and mouse models of CKD.

Case vignette

A 42-year old man with no medical history was admitted to the Nephrology unit for chronic renal insufficiency and hypertension. On admission, vital examination (2016-04-12) showed blood pressure of 179/111 mmHg, proteinuria of 2+, serum creatinine level of 105 $\mu\text{mol/l}$. The patient was diagnosed with CKD1, hypertension (grade 3, high risk), and was given long-term treatment, such as protecting renal function,

improving microcirculation (beraprost sodium), controlling blood pressure, and improving proteinuria. Three months later, the patient was re-admitted for reexamination, and vital examination (2016-07-04) showed blood pressure of 138/82 mmHg, proteinuria of +–, serum creatinine level of 81 $\mu\text{mol/l}$, BUN level of 6.5 mmol/l (Table 1). However, blood pressure slowly increased to 150/110 mmHg since the discontinuation of beprost sodium on July 18, demonstrating BPS as a potent vasodilator. We followed up the patients for 12 months. The data showed that the urinary protein decreased spirally. According to the level of serum creatinine and urea, the patients kept good after discharge (Supplementary fig. S5). It can be seen that the pharmacological mechanism of BPS is dilation of blood vessels, antagonism of renin-angiotensin-induced vasoconstriction, increase of renal blood flow, improvement of renal hypoxia and glomerular filtration rate, and enhancement of renal clearance of toxins. Inhibiting the rising rate of serum creatinine and urea demonstrates that BPS has independent renal protection and delays the progress of the disease.

Materials and methods

Ethics statement

All methods were performed in accordance with the relevant guidelines and regulations. All animal experiments were performed by procedures approved by the Ethics Committee for Animal Research at the Xuzhou Medical University.

Cell culture

The HUVECs were cultured in a modified minimum essential medium (Hyclone, Logan, NY, USA) supplemented with 10% fetal bovine serum (FBS; Hyclone, Logan, UT, USA) and 1% mycillin (Beyotime, Shanghai, China) at 37 °C in 5% CO₂ and 95% air. HUVECs in hypoxia group were cultured for 12 h into an airtight humidified chamber flushed with a gas mixture containing 5% CO₂, 95% N₂, and 1% O₂ at 37 °C. HUVECs in hypoxia + BPS group were cultured with BPS (BEIJING TIDE PHARMACEUTICAL CO., LTD) at 1.0 $\mu\text{mol/l}$. The cells were cultured according to the manufacturer's instructions and the culture medium was changed every 2 or 3 days. HUVECs at passage 3 were used for the following experiments.

Animal models

Thirty-six mice (body weight: 18–22 g, 6- to 8-week-old C57Bl/6J males) were purchased from the Laboratory Animal Centre of Xuzhou Medical University (Jiangsu, China). The animals were maintained in a temperature (22 \pm

Table 1 Renal function in sham, UUU, and BPS groups (mean \pm s.e.m., $n = 6$ each)

	3 days			7 days		
	Sham	UUO	BPS	Sham	UUO	BPS
BUN	7.50 \pm 0.04	7.31 \pm 1.61	5.90 \pm 1.07	7.17 \pm 0.61	7.50 \pm 0.99	6.32 \pm 1.48
Scr	15.62 \pm 0.75	15.67 \pm 2.91	14.09 \pm 1.82	14.95 \pm 0.93	14.97 \pm 1.52	11.59 \pm 1.46*#

Abbreviations: BUN, blood urea nitrogen; Scr, serum creatinine; UUO, unilateral ureteral occlusion; BPS, UUO + beraprost sodium administration

* $P < 0.05$ vs. sham; # $P > 0.05$ vs. UUO

1 °C) and lighting (12 h light–dark cycle) controlled room with free access to food and water. After 1 week of acclimatization, the mice were randomly divided into the three following groups ($n = 16$ in each group): sham-operated mice (sham group), UUO mice intragastrically administered distilled water as a vehicle control (UUO group), and UUO mice treated with BPS (BPS group). To establish the UUO model, a left abdominal incision was made on the mouse after exposure to anesthesia (chloral hydrate 10.0%, 0.003 ml/g intraperitoneal). The left ureter was then ligated with 4–0 silk suture, and the incision was closed in layers. Sham animals were subjected to a similar left abdominal incision, but the left ureter was not ligated. BPS (BEIJING TIDE PHARMACEUTICAL CO., LTD) was administered orally to UUO model at 0.6 mg/kg/d b.i.d., whereas mice in the UUO group were intragastrically administered an equal volume of double-distilled water at the same time every day.

At days 3 and 7 post-surgery, mice from the three groups were sacrificed. Mice blood was obtained from the retro-orbital plexus to measure the concentration of serum creatinine (Scr) and blood urea nitrogen (BUN), then the left kidneys were extracted and washed in saline solution. One part of the kidneys was fixed in 10% formaldehyde for morphological and immunohistochemical staining, while the other part was stored at -80 °C for later PCR and Western blot analysis.

Tube formation assay

Tube formation was performed as previously described [17]. In brief, endothelial cells (1×10^4) were seeded in a 48-well plate coated with 100 μ l of growth factor-reduced Matrigel TM (BD, USA) and incubated with and without varied concentrations of BPS at 0.1, 1.0, and 10.0 μ mol/l for tube stabilization for 24 h at 37 °C. Tube formation was quantified by measuring the total tube loops in five random microscopic fields with a computer-assisted microscope (OLYMPUS, JAPAN).

Renal histology

To evaluate renal morphology, kidney samples were fixed in 10% formaldehyde, embedded in paraffin, sectioned into

4- μ m-thick sections, deparaffinized and then incubated for 15 min in Histochoice. Subsequently, the sections were sequentially incubated for 5 min in 100% alcohol, 95% alcohol, 85% alcohol, 75% alcohol and then stained with hematoxylin-eosin, Masson's trichrome, and picrosirius red. The areas of interstitial fibrosis were detected using Masson's trichrome staining to visualize the collagen fibers, which were stained dark blue and picrosirius red staining, which were stained red. Ten microscopic visual fields of kidney tissues were randomly selected in the sections under high-power magnification ($\times 40$).

FMA

FMA was performed as previously described [18]. Briefly, mice were placed on a surgical heating pad (37 °C) after anesthetized with chloral hydrate (10.0%, 0.003 ml/g intraperitoneal). The abdomen was cut via a midline incision extending from the symphysis pubis to the jugulum. All solutions were prewarmed to 41 °C according to Rafael Kramann et al. One milliliter of heparinized saline followed by 1 ml of 3 M KCl was injected in the beating left ventricle using a vein needle. The right atrium was then cut and the mouse was perfused with 41 °C prewarmed PBS (10 ml), immediately followed by 5 ml of the agarose-microbead mixture (500 ml 0.02 mm FluoSpheres plus 4.5 ml 1% agarose/mouse). The kidneys were excised after the perfusion and carefully placed in a small beaker surrounded by ice for 10 min. Thereafter, the kidneys were fixed in 4% paraformaldehyde on ice for 2 h, then incubated in 30% sucrose in PBS at 4 °C overnight and embedded by optimum cutting temperature (OCT). OCT-embedded kidneys were cryosectioned into 10 μ m sections and mounted on Superfrost slides. Sections were washed in PBS (minutes), stained with 49,6-diamidino-2-phenylindole and mounted in ProLong Gold (Life Technologies). For immunofluorescence staining, selected sections were washed with PBS for 5 min, and then incubated with 5% donkey serum in PBS containing 0.4% Triton-X-100 for 1 h at room temperature before incubation with rabbit anti-CD31 rabbit antibody (1:20, ab28364, abcam), anti-alpha smooth muscle actin rabbit antibody (1:100, ab32575, abcam), anti-alpha smooth muscle actin mouse antibody (1:200, ab7817, abcam), and anti-VE-

cadherin antibody (1:200, ab33168, abcam) at 4 °C for 18 h. Donkey anti-Mouse IgG (H + L) Highly Cross-Adsorbed Secondary Antibody, Alexa Fluor 488 (1:2000, #A-21202, ThermoFisher) and Goat anti-Rabbit IgG (H + L) Highly Cross-Adsorbed Secondary Antibody, Alexa Fluor 594 (1:200, #A-11037, ThermoFisher) were added to the sections and incubated for 2 h at room temperature. Tissue sections were mounted with ProLong Gold Antifade reagent (18255385, Invitrogen). Thereafter, all images were visualized with a confocal laser microscope (FV1000; Olympus, Tokyo, Japan).

Quantitative RT-PCR

RNA from whole tissue samples was isolated using the RNeasy kit (Roche, USA). Quantitative RT-PCR was performed using an ABIPRISM 7300 Sequence Detection System. The final reaction contained template complementary DNA, iTaq SYBR Green Supermix with ROX (Bio-Rad, Hercules, CA, USA) and gene-specific primers (Table 2). The following PCR conditions were used: 50 °C for 2 min and 95 °C for 10 min, followed by 40 cycles for 30 s at 95 °C, 45 s at 60 °C, and 30 s at 72 °C. GAPDH was used as an internal control. The cycle threshold values of GAPDH and other specific genes were acquired after PCR. The normalized fold expression was obtained using the $2^{-\Delta\Delta CT}$ method. The results were expressed as the normalized fold expression for each gene.

Western blotting

Kidney tissue samples were lysed in RIPA and PMSF (RIPA:PMSF = 100:1) on ice 30 min and then centrifuged at

12,000 rpm for 15 min at 4 °C. After the protein samples were heated in boiling water for 5 min, approximately 150 µg of total protein was loaded on 10% or 12% sodium dodecyl sulfate-polyacrylamide (SDS) gels and transferred to a polyvinylidene difluoride (PVDF) membrane by electroblotting. Non-specific binding was blocked by incubating the membrane in 3% bovine serum albumin (BSA) for 1 h at room temperature. The membrane was then incubated overnight at 4 °C with primary antibodies against TGF-β1 (1:1000, Abcam), UCP2 (1:800, Abcam), NT (1:200, SANTA CRUZ), MCP-1 (1:2000, Abcam), IL-6 (1:500, ABclonal), HIF1-α (1:500, Proteintech), and VEGF (1:200, Abcam), followed by an incubation with ECL secondary antibodies. The signal was detected with ImageQuant LAS 4000 mini and was quantified by beta actin.

Statistical analyses

Data are presented as the mean ± SD, and statistical analysis was performed with Graph-Pad Prism software, version 6.0c. Comparisons between groups were analyzed by one-way analysis of variance (ANOVA) with Dunnett's post hoc test or post hoc Bonferroni correction. A *P* value less than 0.05 was considered statistically significant.

Results

BPS regulates capillary-like formation in vitro

A matrigel-based tube formation assay was performed to assess the ability of HUVEC to form an organized tubular network (Fig. 1a). In the normal culture medium, rarely formed capillary-like structures was observed. However, BPS treatment leads to a significant increase in the number of tube formation (Fig. 1b). These results demonstrated that BPS plays an important role on angiogenic activity.

BPS regulates endothelial junctions in vitro

Vascular endothelial cadherin (VE-cadherin) is specifically represent for endothelial adherens assembly and barrier architecture. HUVECs in the normoxia group showed consistent expression of VE-cadherin at cell–cell contacts. However, this expression followed a sawtooth distribution typically associated with the lack of tight junctions in the hypoxia group. The proteins of VE-cadherin that were regularly distributed on the cell membrane were dispersed in the cytoplasm and nucleus after 12 h hypoxia condition. Conversely, in the BPS group, VE-cadherin at regions of cell–cell contact became more abundant and the morphology of endothelial cells tends to be normal compared with those cultured under hypoxia conditions (Fig. 1c).

Table 2 The sequences for the primers

Gene	Primer sequences
GAPDH	5'-ACCACTTGGTATCGTGGAAGG-3' 5'-GCCATCACGCCACAGTTTC-3'
VEGF	5'-GCTGTAACGATGAAGCCCTG-3' 5'-GACCCTTXXCCTTXXATCGA-3'
TGFβ1	5'-TCGCTTTGTACAACAGCACC-3' 5'-ACTGCTTCCCGAATGTCTGA-3'
HIF-1α	5'-CTCACCAGACAGAGCAGGAA-3' 5'-AAGGGAGCCATCATGTTCCA-3'
MCP1	5'-CCACTCACCTGCTGCTACTCATT-3' 5'-CTGCTGCTGGTGATCCTCTT GTAG-3'
IL-6	5'-ACGGCCTTCCCCTACTTCACA-3' 5'-CCACGATTCCCAGAGAACA-3'
UCP2	5'-CTCCCAATGTTGCCCGTAAT-3' 5'-GTGAAGTGGCAAGGGAGGTC-3'

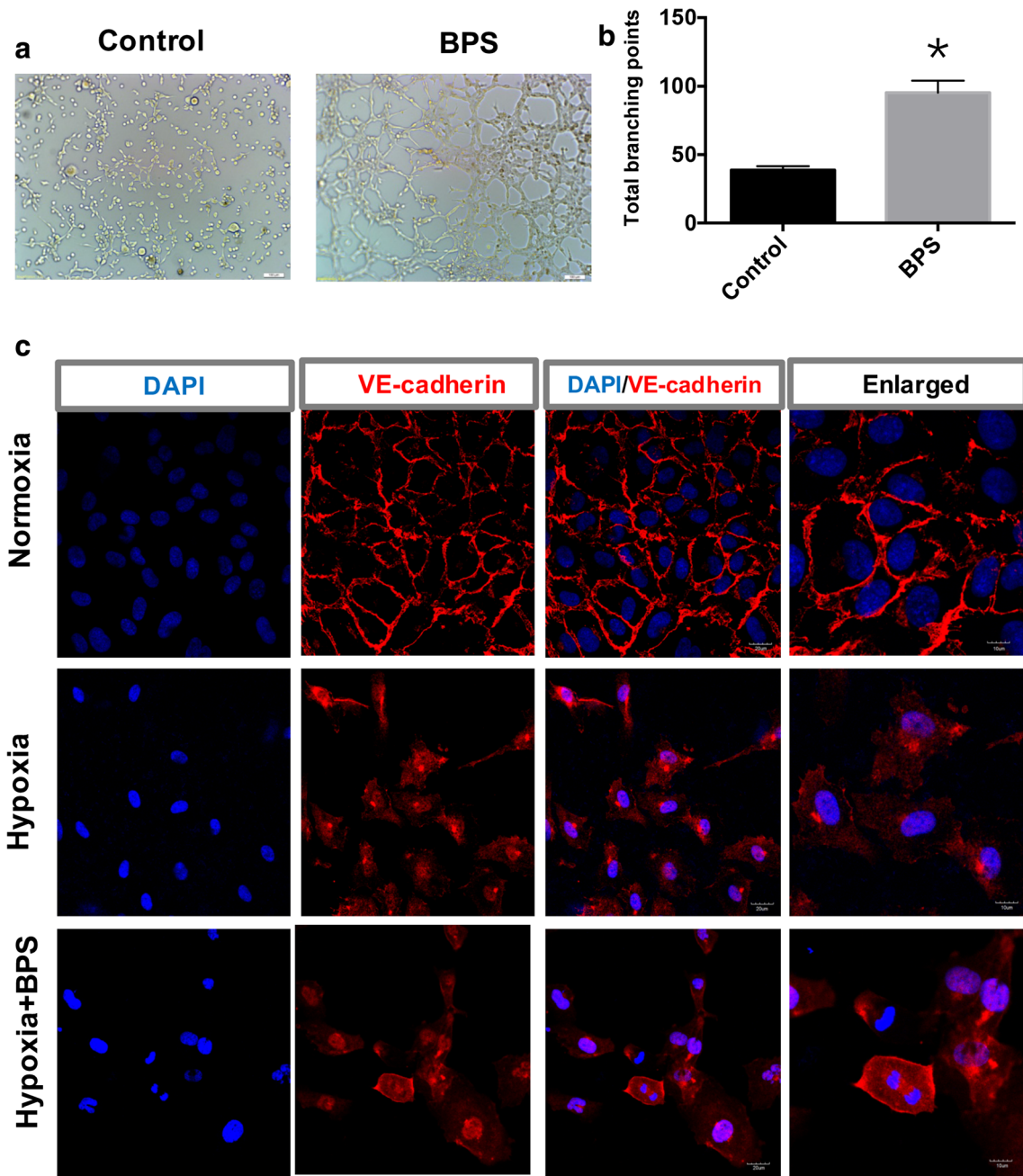


Fig. 1 BPS regulates capillary-like formation and endothelial junctions in vitro. HUVEC were seeded on the matrigel matrix and transfected with BPS or negative control. The tube-like structures were observed using a microscopy 24 h after transfection. **a** Representative images and quantification of the organization into capillary-like structures in control and BPS groups. **b** The bar graph shows a significant increase of the number

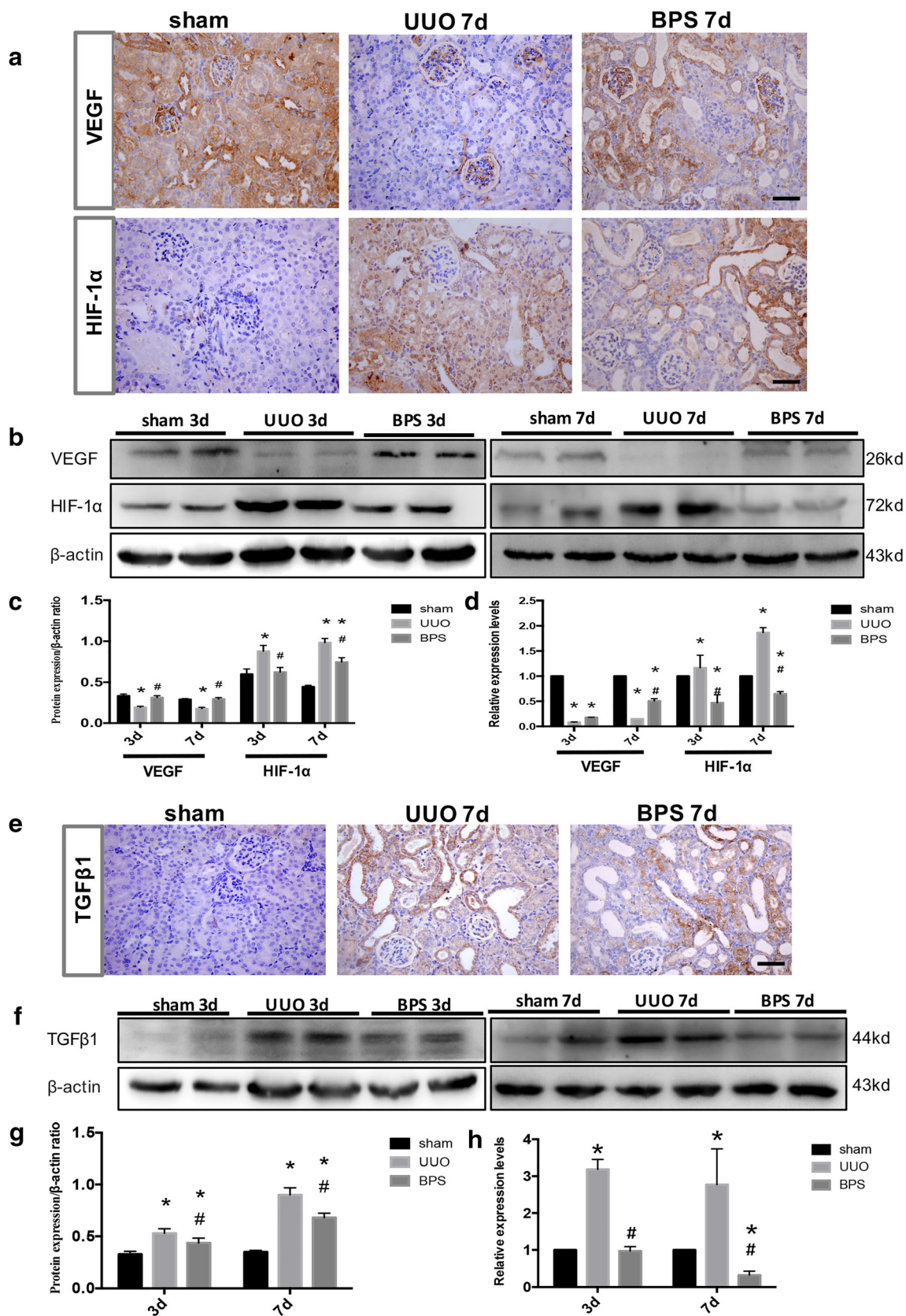
of branches in the BPS group compared with control ($n = 6$). **c** The expression and the distribution of VE-cadherin (red) were regulated and high expressed in the normoxia group, but was reduced and rearranged in the hypoxia group. The morphology of endothelial cells and cell–cell contact was slightly recovered in the BPS group. Nuclei were stained with DAPI (blue) ($n = 6$)

Gene expression and protein expression levels of vascular endothelial growth factor (VEGF) and hypoxia-inducible factor-1 α (HIF-1 α)

The expressions of VEGF mRNA at different time points after UUO were assessed by q-PCR. As shown in Fig. 2d, VEGF mRNA was significantly reduced after UUO compared with

that in the sham group, and increased after BPS treatment. Immunohistochemical staining and Western blot analysis revealed similar trends in VEGF protein levels to those observed in the RT-PCR results (Fig. 2a–c). These results suggest that BPS may promote angiogenesis in obstructed kidneys.

HIF-1 α gene expression increased owing to the rarefaction of the PTC in the UUO group compared with that in the sham



◀ **Fig. 2** Comparisons of VEGF, HIF-1 α and TGF β 1 expressions in each group by Western blot analysis and qRT-PCR. **a** VEGF staining was decreased in the UUO group compared with that in the sham group at day 7 post-surgery, whereas the staining was increased in the BPS group compared with that in the UUO group. HIF-1 α expression was increased in the UUO group, while was decreased in the BPS group compared with the UUO group. Bar = 20 μ m. **b** Representative (2 bands shown per group) immunoblotting of VEGF and HIF-1 α . **c** Graphic presentation of the quantitative data demonstrated that VEGF protein expression was decreased in the UUO group compared with the sham group at both day 3 and 7 post-surgery, whereas was increased in the BPS group compared with the UUO group; HIF-1 α expression was increased in the UUO group compared with that in the sham group, while the expression was decreased in the BPS group compared with the UUO group. Relative protein levels after normalization with β -actin are reported. **d** VEGF mRNA expression levels were decreased in the UUO group and increased in the BPS group at day 7. There were no significant differences in VEGF mRNA expression at day 3 post-surgery between the UUO and BPS groups. The HIF-1 α mRNA expression was elevated in the UUO group and decreased in the BPS group at days 3 and 7. **e-h** The fibrotic marker TGF β 1 protein and mRNA expressions were elevated in the UUO group and decreased in the BPS group at each time point. (* $P < 0.05$ vs. sham group; # $P < 0.05$ vs. UUO group). Of note, data represent $n = 10$ mice in each group

group. However, compared with the UUO group, the BPS group exhibited dramatically decreased HIF-1 α gene expression. Immunohistochemical staining and Western blot analysis confirmed that the increase in HIF-1 α seen in UUO models was substantially decreased in BPS group at each time point (Fig. 2a–c). These results demonstrate that BPS treatment alleviates the hypoxic conditions associated with obstructed kidney.

Gene expression and protein expression levels of transforming growth factor- β 1 (TGF- β 1)

Although increased TGF- β 1 gene and protein expressions were detected in the obstructed kidney, demonstrating the progression of renal fibrosis. Conversely, gene and protein expressions were expressed at lower levels in the UUO mice treated with BPS, compared with the UUO group (Fig. 2e–h). In brief, our data indicated that renal fibrosis was significantly alleviated after the treatment of BPS in established UUO models.

Gene expression and protein expression levels of nitrotyrosine (NT), anti-uncoupling protein 2 (UCP2) expression levels

To further explore the mechanism underlying the antifibrotic effect of beraprost sodium, we examined whether the therapeutic effect of BPS on renal fibrosis was mediated by suppressing oxidative stress. As shown in Fig. 3d, low UCP2 gene expression levels were detected in the sham group. However, the UCP2 gene expression was dramatically induced in the obstructed kidney at days 3 and 7, while decreased after BPS treatment. Similar results were obtained

by immunohistochemical staining and Western blot analysis (Fig. 3a–c). Marked upregulation of NT and UCP2 protein was observed in the fibrotic kidneys after UUO, whereas they were decreased in the BPS group compared with those in the UUO group. These data demonstrate the superior anti-oxidative effect of BPS.

Gene expression and protein expression levels of monocyte chemoattractant protein 1 (MCP1) and interleukin-6 (IL-6)

Inflammation is believed to be an important factor in the pathogenesis of renal fibrosis. We investigated the hypothesis that the protective action of BPS is attributed to its anti-inflammatory effect. As shown in Fig. 3h, the mRNA expression levels of MCP1 and IL-6 were significantly elevated at different time points in the obstructed kidneys compared with the control mice. However, BPS treatment significantly prevented these increases. Consistent with the genetic analysis, treatment with BPS-induced parallel decreases in the protein expression of the inflammatory markers in the UUO group (Fig. 3e–g). These data demonstrate the anti-inflammatory capability of BPS.

Peritubular capillary changes detected by fluorescence microangiography (FMA)

To observe peritubular capillary changes in each group, we applied fluorescence microangiography (FMA) approach combined with MATLAB analysis of peritubular capillary size and density (Fig. 4). Obstructed kidney led to a reduction in capillary number, total perfused area compared with the sham group. However, the total area and total number of capillaries were significantly increased after the administration of BPS compared with the UUO group. The individual capillary cross-sectional area in UUO group was smaller than that in the sham group, but the treatment of BPS has no good effect on it. Meanwhile, there was no differences of individual capillary perimeter within the three groups, indicating that peritubular capillary size did not significantly change after UUO model and BPS treatment. The higher magnification of the far right images showed that capillaries surrounded by CD31⁺ endothelial cells in the UUO group appeared a reduced luminal FMA signal, indicating that these capillaries lack perfusion, but increased FMA perfused area was shown in the BPS group. All microvascular characteristics were analyzed by MATLAB-based script (Supplementary fig. S1). Staining and quantification of α -SMA protein expression showed a significant increase in the UUO group compared with the sham group and BPS treatment inhibited the fibrotic progress (Fig. 5). These results provide more direct and precise evidence that BPS could promote the renal microcirculation and subsequently alleviate renal interstitial fibrosis.

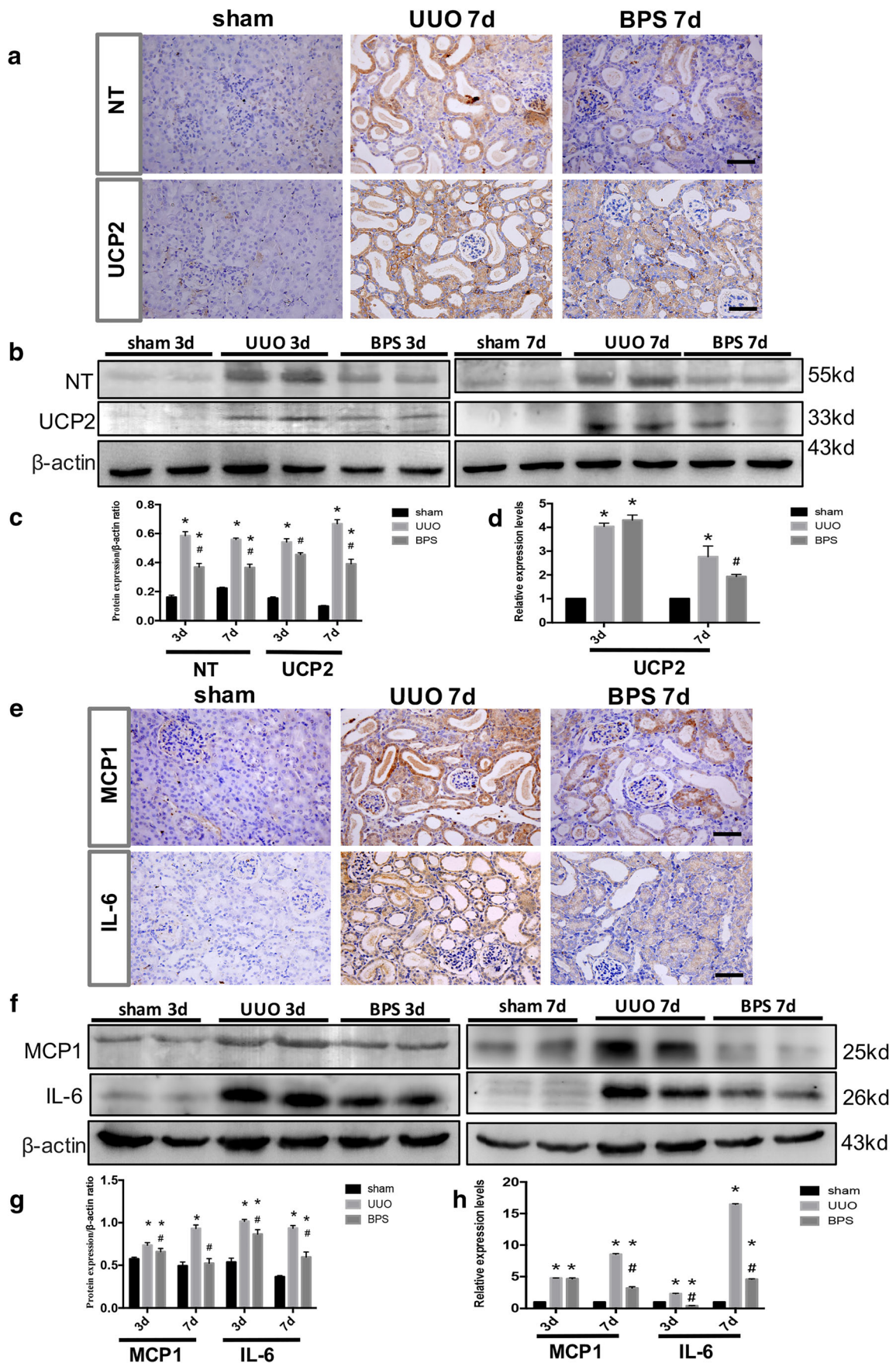


Fig. 3 Western blot analysis of nitrotyrosine (NT), UCP2, MCP1, and IL-6 and comparisons of UCP2, MCP1, and IL-6 mRNA expressions in each group by qRT-PCR. **a** NT, UCP2 staining was increased in the UUO group at day 7 post-surgery, while were decreased in the BPS group. Bar = 20 μ m. **b** Representative (2 bands shown per group) immunoblotting of NT and UCP2. **c** Graphic presentation of the quantitative data demonstrated that NT and UCP2 protein expressions were elevated in the UUO group at day 3 and 7 post-surgery compared with that in the sham group and decreased in the BPS group compared with that in the UUO group. **d** The mRNA expression levels of UCP2 were upregulated in the UUO group at days 3 and 7, whereas the levels were downregulated in the BPS group. **e** MCP1 and IL-6 staining were increased in the UUO group, whereas were decreased in the BPS group. Bar = 20 μ m. **f** Representative (2 bands shown per group) immunoblotting of MCP1 and IL-6. **g** Graphic presentation of the quantitative data demonstrated that MCP1 and IL-6 protein expressions were increased in the UUO group compared with that in the sham group at day 3 and 7 post-surgery, whereas were suppressed by BPS treatment. There were no significant differences in VEGF protein expression at day 3 post-surgery between the UUO and BPS groups. **h** The mRNA expression of MCP1 and IL-6 were elevated in the UUO group and decreased in the BPS group. VEGF mRNA expression at day 3 post-surgery did not significantly change after BPS administration compared with the UUO group. (* $P < 0.05$ vs. sham group; # $P < 0.05$ vs. UUO group). Of note, data represent $n = 10$ mice in each group

Renal morphology

Renal histology was investigated using hematoxylin-eosin, Masson's trichrome, and picrosirius red staining. As shown in Fig. 6a, there was no significant histological abnormality in the sham group. After unilateral ureteral occlusion, severe morphological lesions and extracellular matrix (ECM) production were detected. However, compared with the UUO group, renal pathological alterations and collagen deposition were substantially improved after administration of therapeutic BPS.

BPS alleviates EndMT in UUO models

Immunostaining was performed to identify cells undergoing EndMT on the basis of coexpression of endothelial cell (CD31) and myofibroblast (α -SMA) markers. Samples taken from the sham-operated group showed the presence of both CD31⁺ endothelial cells and resident α -SMA⁺ cells, but no double-labeled cells were evident (Fig. 6d). Obstructed kidney exhibited a decrease of CD31⁺ endothelial cells and the coexpressing CD31⁺ α -SMA⁺ cells were apparent, indicating an active role for EndMT progression in the fibrotic kidneys after UUO. By contrast, higher numbers of α -SMA⁺ myofibroblasts, but fewer CD31⁺ endothelial cells in the BPS group were detected compared with the UUO group, and CD31⁺ α -SMA⁺ EndMT cells correlated with interstitial fibrosis were downregulated. These findings suggest that EndMT may account for a considerable portion of the fibroblasts in UUO models, but BPS can mitigate EndMT progression.

Renal function

To further investigate whether BPS could improve renal function, serum creatinine (Scr) and blood urea nitrogen (BUN) obtained from the retro-orbital plexus were assessed. BUN at different time points and Scr at day 3 were not significantly different among the groups (Table 1, $P > 0.05$ each), but serum creatinine was decreased in the BPS group compared with the UUO group at day 7 (Table 1, $P < 0.05$ each).

Discussion

In this study, we found that the rarefaction of peritubular capillaries accompanied by severe hypoxia were induced by the obstructive kidney, which escalating the extent of renal injury and impede recovery, leading to renal fibrosis. BPS treatment could mitigate the development of renal interstitial fibrosis that were likely primarily attributed to the inhibition of inflammation and oxidative stress and further suppressing EndMT.

Chronic kidney disease (CKD) has received increased attention as a public health problem globally [19]. A recent national cross-sectional study in China showed that the overall prevalence of CKD was 10.8% [20]. Although numerous researchers have made great efforts to explore the mechanisms of CKD over the last several decades, the current methods for CKD treatment are still ineffective. Therefore, a better understanding of the pathogenesis of CKD and methods to arrest the progression of renal fibrosis are urgently needed.

Yokoyama et al. demonstrated that endogenous PGI₂ played a significant role in the renal development and functional preservation, since prostacyclin synthase knockout mice develop severe renal damage [21]. BPS, a stable PGI₂ analog, has potent vasodilation effect in a variety of organs [22]. BPS is clinically used in patients with chronic arterial occlusive disease and pulmonary arterial hypertension; it is also used in CKD patients through improving regional blood flow. However, the potential mechanism of BPS against renal fibrosis remains to be elucidated.

Several studies demonstrated that progressive renal fibrosis are characterized by an early and progressive decrease in relative blood volume and microvascular density in different models [6]. These peritubular capillaries deliver oxygen to the kidney tissue, but loss of capillaries contributes to focal hypoxia, inducing an injury cascade with oxidative and inflammatory effects, which damage endothelial cells and induce endothelial cells-to-myofibroblast transition. These changes in turn exacerbate PTCs rarefaction, stimulating the expansion of hypoxic areas and creating a vicious cycle favoring fibrogenesis [23–26]. Therefore, we explored if BPS could alleviate renal injury through promoting microcirculation. First, we showed BPS treatment in endothelial cells result in increased capillary-like structure formation compared

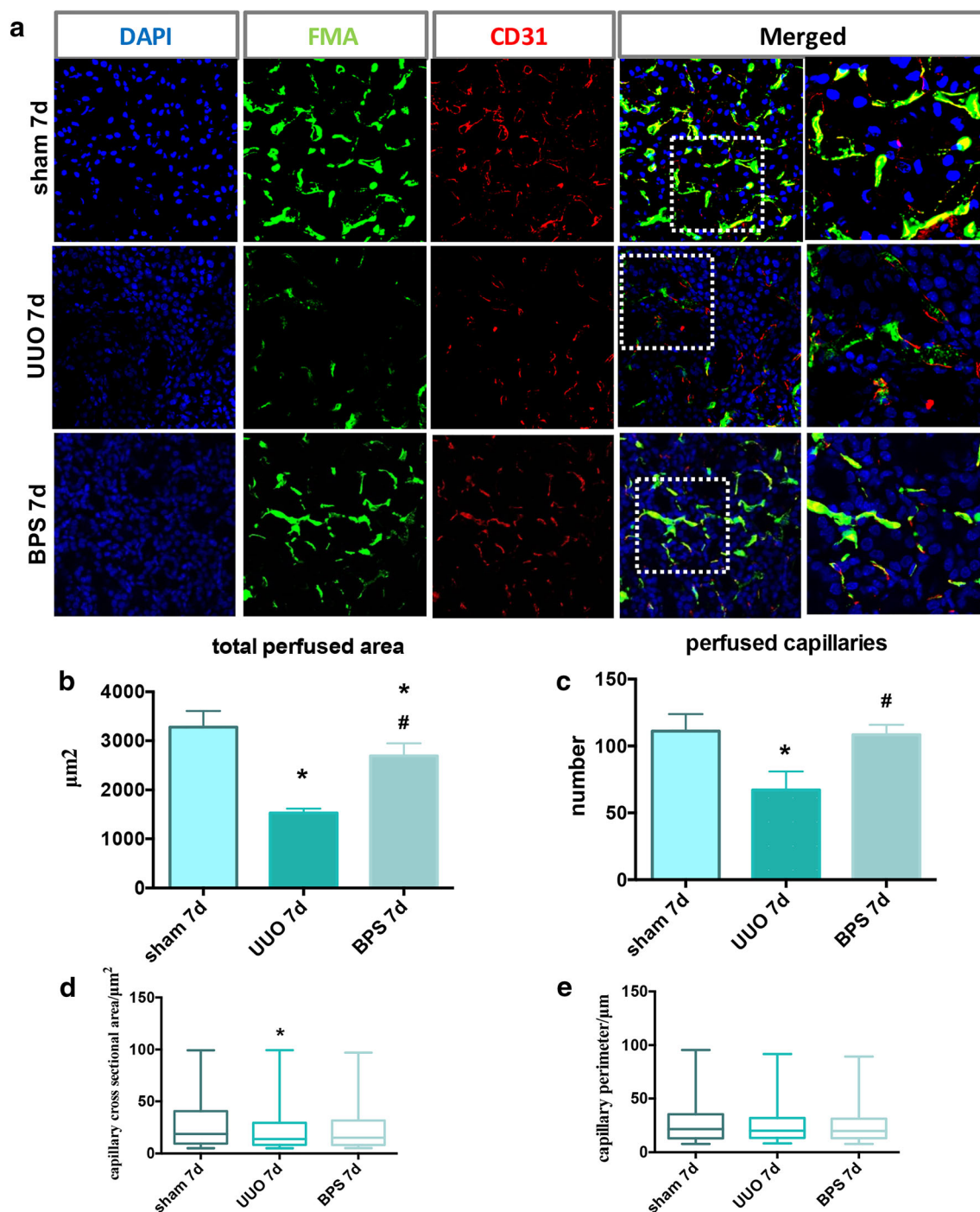


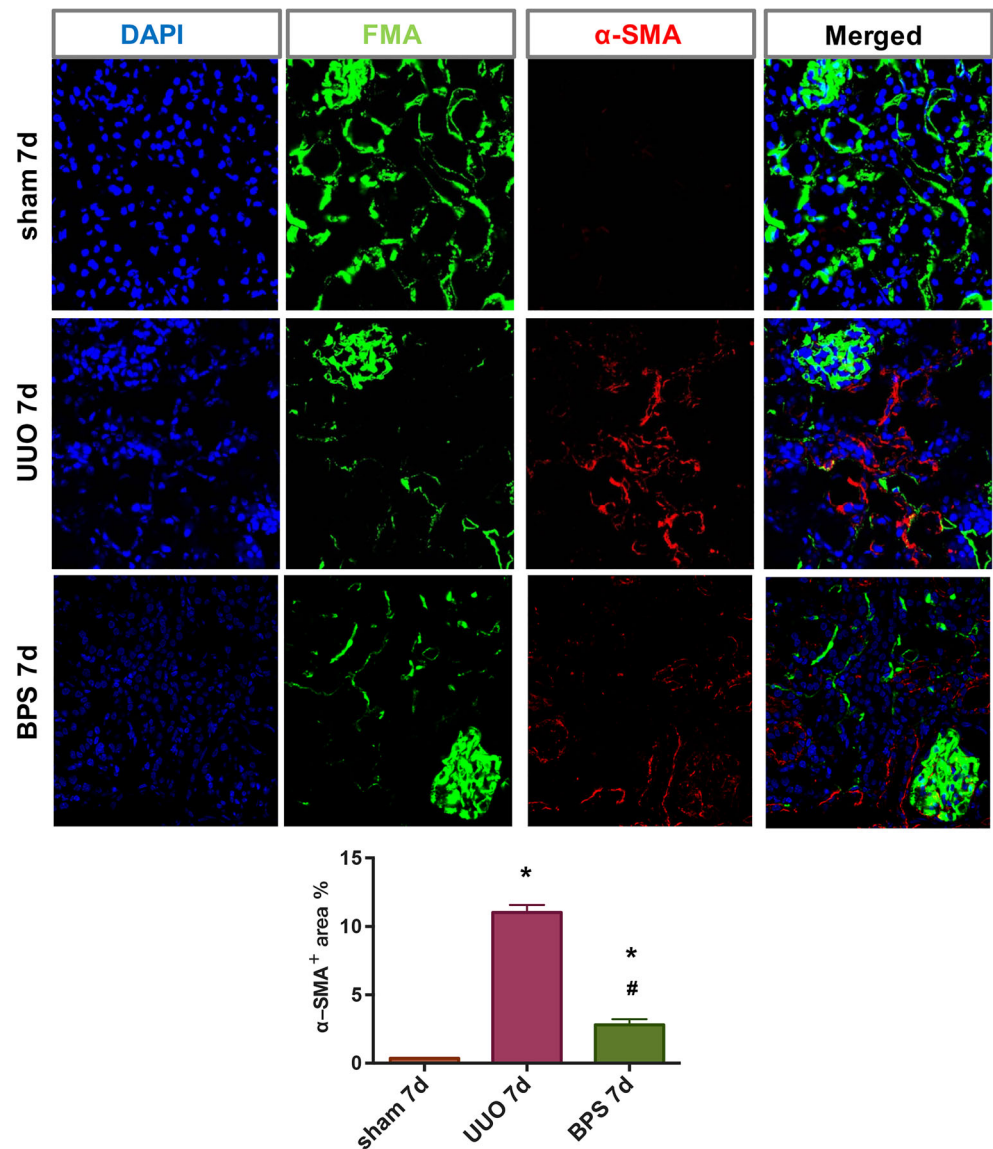
Fig. 4 Fluorescence microangiography (FMA) (**a–c**) The green FMA solution injected after sham surgery and UUO 7d, surrounding with CD31 immunostaining (expressed on the surface of endothelial cells), demonstrates loss of capillaries in response to obstructed kidney. Reduced capillary number and perfused area were restored after BPS treatment. Representative images in the box were presented by higher magnification, demonstrating that capillaries surrounded by CD31⁺ endothelial cells in the UUO group do not appear a luminal FMA signal

indicating that these capillaries lack perfusion, but increased FMA perfused area was shown in the BPS group. **d, e** The individual capillary cross-sectional area in UUO group was smaller than that in the sham group, but BPS treatment has no good effect on it. There were no differences of individual capillary perimeter within the three groups. (* $P < 0.05$ vs. sham group; # $P < 0.05$ vs. UUO group). Of note, data represent $n = 6$ mice in each group

endothelial cells without BPS in vitro, suggesting that BPS contributes to angiogenesis and vessel remodeling process. Additionally, cell–cell interactions are barrier to maintain

homeostasis of blood vessels. Damage to endothelial cell–cell junctions results in increased microvascular permeability. Some leukocytes migrate through the endothelial cells into the

Fig. 5 Fluorescence microangiography (FMA) of PTCs and immunofluorescence staining of α -SMA in the renal mesenchyme and quantification revealed induction of interstitial fibrosis after unilateral ureteral obstruction compared with the sham group. However, BPS suppressed fibrotic expressions. (* $P < 0.05$ vs. sham group; # $P < 0.05$ vs. UUO group). Of note, data represent $n = 6$ mice in each group



interstitial compartment, contributing to the swelling of the interstitial space and compression of the microvasculature to further extend the distance of oxygen diffusion and reduce nutritive flow. VE-cadherin is specifically represent for endothelial adherens assembly and barrier architecture. We observed BPS could remodeling disrupt endothelial cell–cell junction caused by hypoxia by detecting the increased expression of VE-cadherin, suggesting a benefit effect of BPS in improving microcirculation in vitro.

To further investigate whether BPS had any impact on renal microvascular in vivo, we give UUO mice intragastrically administered of BPS. To date, microvascular density is measured by CD31 antigens immunostaining which calculate the surface area of endothelial cells or genetic labeling (such as Tie 2) [27], whereas the actual capillary lumen could not be estimated. In our study, we use the novel technique, FMA, which relies on low-melting-point agarose added with

FluoSpheres to provide a microangiogram that can be visualized with a confocal laser microscope [18]. It should also enable us analyzing total perfused capillary area, peritubular capillary number, and individual capillary cross-sectional area and perimeter by using MATLAB software, which could automatically generates analysis of the microvasculature by using MATLAB script [18]. PTC-positive areas, which were determined based on CD31 immunostaining in present study, showed that the PTCs were damaged in the UUO group. Meanwhile, perfused FMA+ capillary area showed lack perfusion in obstructed kidneys. The rarefaction of the PTCs in turn results in tissue hypoxia, which was suggested by the upregulation of HIF-1 α . Our study showed that BPS treatment could restore renal blood vessels, stimulate an augment in PTC density, and relieve tissue hypoxia. Under hypoxia, renal endothelial cells undergo endothelial-mesenchymal transitions. These cells can migrate to the interstitium and

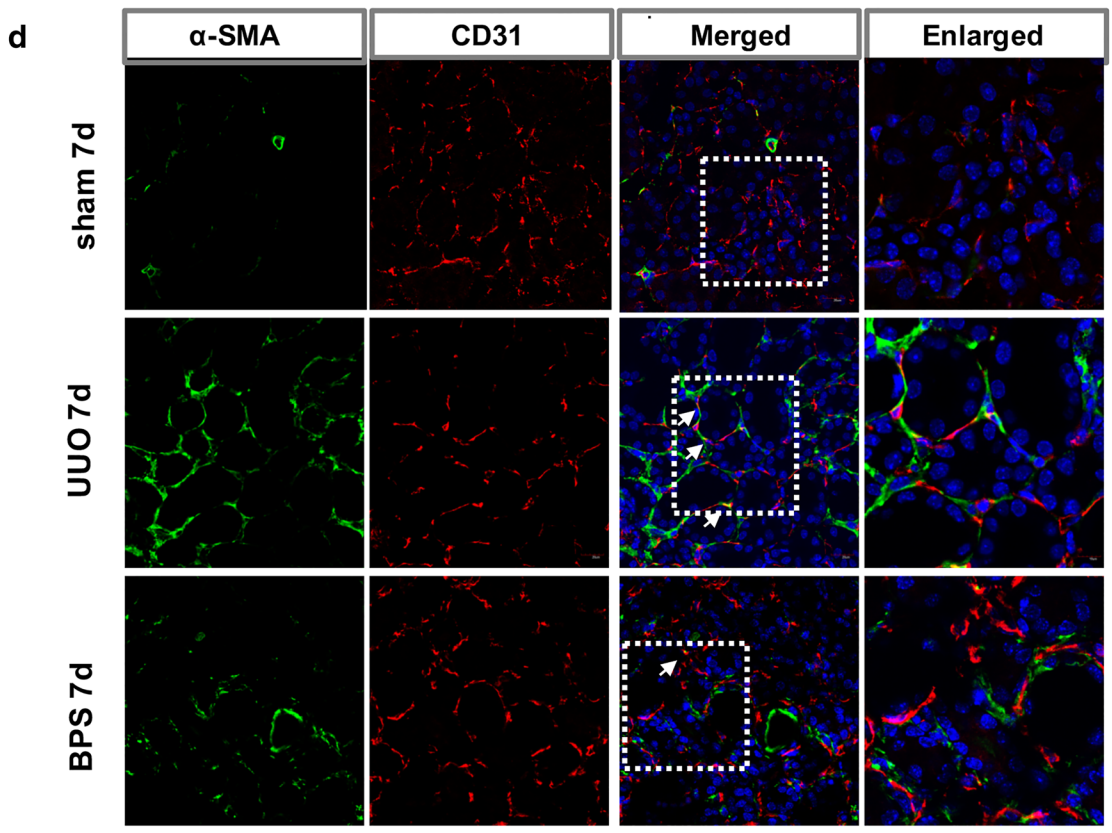
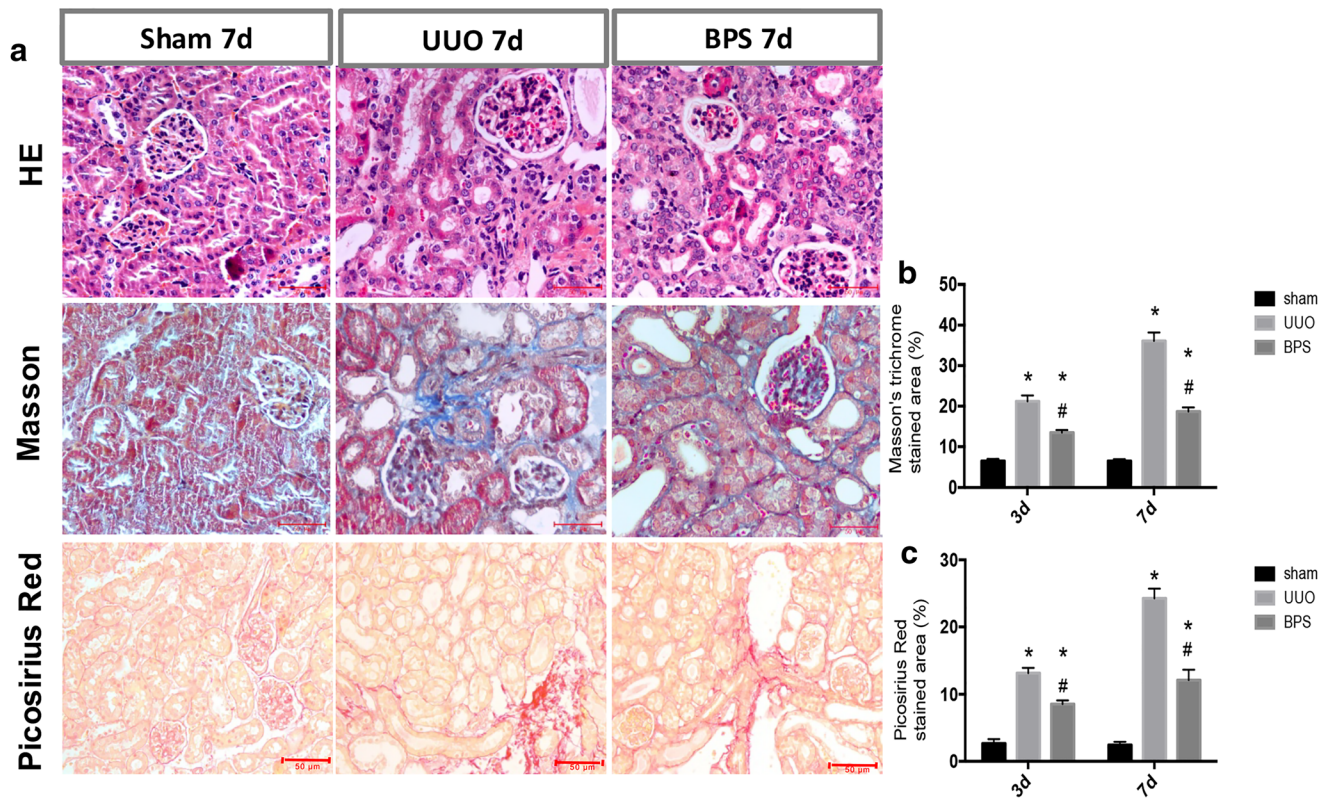


Fig. 6 BPS improves the morphology of renal histology and inhibits EndMT progression in the obstructed kidney. **a** Representative micrographs of hematoxylin-eosin, Masson's trichrome and picrosirius red staining demonstrate histological changes in the 7 days post-surgery groups. **b, c** Quantification of renal interstitium areas in each group on both 3 and 7 days post-surgery. Fibrosis increased in UUO compared with sham, decreased in the BPS group compared with the UUO group. Bar = 20 μm . (* $P < 0.05$ vs. sham group; # $P < 0.05$ vs. UUO group). **d** There were no evident two-color immunofluorescence identifies EndMT cells that coexpress endothelial cells (CD31, red) and myofibroblast cells (α -SMA, green) shown in the sham group. EndMT progression were increased in the UUO group and decreased in the BPS group, indicating by the coexpression of CD31⁺ α -SMA⁺. White arrows indicate positive coexpressing staining. Nuclei were stained with DAPI in blue. Bar = 20 μm . Of note, data represent $n = 6$ mice in each group

differentiate into myofibroblasts and promote ECM production, such as collagen [28]. These data suggest that the BPS treatment has the ability of angiogenesis and subsequently alleviate the degree of renal fibrosis with the underlying mechanisms of anti-inflammatory and anti-oxidative effects.

BPS treatment relieving hypoxia and remaining vessels subsequently result in reduced renal inflammation and oxidative stress in UUO model. Previous studies [29, 30] have suggested that the renal fibrosis induced by obstructed kidneys is characterized by inflammatory cell recruitment, macrophage infiltration, and increased proinflammatory cytokines. Secretion of a large amount of cytokines activates not only leukocyte rolling and adhesion but also cells present in the microenvironment, such as fibroblasts and myofibroblasts, which contributes to renal fibrogenesis [24, 31]. In this study, our results showed that UUO models characterized by distinct increased expression of proinflammatory cytokines such as MCP1 and IL-6, both of which were ameliorated upon BPS administration, that may determine the reduction of extracellular matrix accumulation. In addition, oxidative stress played a major role in sustaining fibrosis in obstructed kidneys. The expression levels of oxidative stress markers were observed in our study, including NT [32], used as an indirect indicator of peroxynitrite and UCP2 [33], known as a mitochondrial inner membrane protein that regulates proton conductance, which are both upregulated in UUO models. However, compared with the UUO group, the kidneys treated with BPS exhibited markedly reduced oxidative effects, which suggested that BPS ameliorated renal fibrosis through anti-oxidative effects.

A growing number of studies have suggested that renal fibrosis due to oxidative stress and inflammation are associated with ECM deposition. Oxidative stress and inflammation can activate apoptosis of renal endothelial cells and tubular epithelial cells [34], which induce EndMT and epithelial-mesenchymal transition (EMT) and finally facilitate extracellular matrix deposition [2]. Furthermore, the excessive ROS production [35] leads to a reduction in respiratory chain function in mitochondria and eventually results in activating EndMT and EMT during UUO-induced renal interstitial

fibrosis. As immunostaining showed, endothelial cells undergoing EndMT in chronic kidney disease were observed by confocal microscopy, indicating that injured endothelial cells can transform into myofibroblasts. However, this EndMT process was inhibited by BPS treatment by noting that fewer CD31⁺ endothelial cells and α -SMA⁺ myofibroblasts colocalized in areas of renal interstitium. These results demonstrate that BPS can lighten the progress of EndMT caused by oxidative stress and inflammation.

To further investigate whether BPS could improve renal function, we measured Scr and BUN obtained from the retro-orbital plexus and found that Scr were downregulated in BPS group compared with the UUO group, suggesting a potential renal protection of BPS. However, no significant differences were detected in BUN among three groups, but the reason is unclear. Simultaneously, TGF- β 1 and α -SMA, play major role in fibrosis, were also observed reducing after BPS administration, which is associated with its anti-inflammatory actions and anti-oxidative effects.

Several studies reported that BPS could also effectively reduce the blood pressure of model mice [22, 36, 37]. Therefore, we speculated that the therapeutic effect of BPS on renal fibrosis may due to its potential contribution of a general blood pressure lowering effect. Hypertension, which is accompanied by functional and structural alterations in microvessels, is a risk factor leading to renal fibrosis [38, 39]. Inflammatory cell recruitment, macrophage infiltration, and increased proinflammatory cytokines were observed during the progression of renal fibrosis in the salt-sensitive hypertension (SSHT) model [40]. Inflammatory activation results in apoptosis of endothelial cells and increase exposure of endothelial adhesion molecules. Our study also found that coronary artery stenosis (CAS) accompanied by hypertension exacerbates capillary loss and consequently tissue inflammation and oxidative stress, and it synergistically magnifies kidney interstitial fibrosis [41]. Therefore, BPS may inhibit renal inflammation, decrease renal oxidative stress through its potential vasodilation effect, and further prevent renal interstitial fibrosis.

In summary, BPS, has potent vasodilating effect in various organs, was shown renal function preservation and fibrosis alleviation in our study. We show here that BPS can restore damaged peritubular capillaries accompanied by oxidative and inflammatory outburst, and subsequently relieving EndMT and ECM deposition. We also found that microvascular injury could be detected by new technical FMA, which serve as a useful functional readout for therapeutics targeting vascular survival. These results demonstrate the potent therapeutic of BPS in improving kidney failure and fibrosis after injury.

Acknowledgements This study was supported by funding from the National Natural Science Foundation of China (81270769); the Jiangsu

Provincial Natural Science Foundation (BK20161172); the Jiangsu Provincial Commission of Health and Family Planning (2016103003); a project of the Jiangsu Provincial Commission of Health and Family Planning (H201628); a project of Qing Lan of Jiangsu Province; a project of “Liu Ge Yi” of Jiangsu Province (LGY2016043); the project of “Liu Da Ren Cai Gao Feng” of Jiangsu Province, China (WSN-113, 2010-WS043); the Technology Development Foundation of Kuitun City (201134); the Jiangsu Overseas Training Program for University Prominent Young and Middle-aged Teachers and Presidents; and Shi Er Wu Ke Jiao Xing Wei Key Medical Personnel of Jiangsu Province (RC2011116); a school class project of Xuzhou Medical University (2017KJ13); Municipal key research and development project of Xuzhou (KC18212); a project of Jiangsu Provincial Post Graduate Innovation Plan (KYCX17_1708, SJCX17_0560, KYCX18-2178, SJCX18_0715).

Compliance with ethical standards

Disclosures None.

References

- Campanholle G, Ligresti G, Gharib SA, Duffield JS (2013) Cellular mechanisms of tissue fibrosis. 3. Novel mechanisms of kidney fibrosis. *Am J Phys Cell Phys* 304(7):C591–C603
- Fu H, Tian Y, Zhou L, Zhou D, Tan RJ, Stolz DB, Liu Y (2017) Tenascin-C is a major component of the fibrogenic niche in kidney fibrosis. *J Am Soc Nephrol* 28(3):785–801
- Ligresti G, Nagao RJ, Xue J, Choi YJ, Xu J, Ren S, Aburatani T, Anderson SK, MacDonald JW, Bammler TK, Schwartz SM, Muczynski KA, Duffield JS, Himmelfarb J, Zheng Y (2016) A novel three-dimensional human peritubular microvascular system. *J Am Soc Nephrol* 27(8):2370–2381
- Long DA, Norman JT, Fine LG (2012) Restoring the renal microvasculature to treat chronic kidney disease. *Nat Rev Nephrol* 8(4):244–250
- Ohashi R, Shimizu A, Masuda Y, Kitamura H, Ishizaki M, Sugisaki Y, Yamanaka N (2002) Peritubular capillary regression during the progression of experimental obstructive nephropathy. *J Am Soc Nephrol* 13(7):1795–1805
- Babickova J, Klinkhammer BM, Buhl EM, Djurdjaj S, Hoss M, Heymann F, Tacke F, Floege J, Becker JU, Boor P (2017) Regardless of etiology, progressive renal disease causes ultrastructural and functional alterations of peritubular capillaries. *Kidney Int* 91(1):70–85
- Li S, Zhao Y, Wang Z, Wang J, Liu C, Sun D (2018) Transplantation of amniotic fluid-derived stem cells preconditioned with glial cell line-derived neurotrophic factor gene alleviates renal fibrosis. *Cell Transplant* 28:963689718815850
- Tanaka T, Nangaku M (2013) Angiogenesis and hypoxia in the kidney. *Nat Rev Nephrol* 9(4):211–222
- Eardley KS, Kubal C, Zehnder D, Quinkler M, Lepenies J, Savage CO, Howie AJ, Kaur K, Cooper MS, Adu D, Cockwell P (2008) The role of capillary density, macrophage infiltration and interstitial scarring in the pathogenesis of human chronic kidney disease. *Kidney Int* 74(4):495–504
- Chuang ST, Kuo YH, Su MJ (2015) KS370G, a caffeamide derivative, attenuates unilateral ureteral obstruction-induced renal fibrosis by the reduction of inflammation and oxidative stress in mice. *Eur J Pharmacol* 750:1–7
- Holterman CE, Read NC, Kennedy CR (2015) Nox and renal disease. *Clin Sci (Lond)* 128(8):465–481
- Walther CP, Navaneethan SD (2017) Inflammation as a therapeutic target to improve vascular function in kidney disease. *J Am Soc Nephrol* 28(3):723–725
- Xiao X, Du C, Yan Z, Shi Y, Duan H, Ren Y (2017) Inhibition of necroptosis attenuates kidney inflammation and interstitial fibrosis induced by unilateral ureteral obstruction. *Am J Nephrol* 46(2):131–138
- Nagaya N, Uematsu M, Okano Y, Satoh T, Kyotani S, Sakamaki F, Nakanishi N, Miyatake K, Kunieda T (1999) Effect of orally active prostacyclin analogue on survival of outpatients with primary pulmonary hypertension. *J Am Coll Cardiol* 34(4):1188–1192
- Matsumoto T, Iwasa K, Kyuragi R, Honma K, Guntani A, Ohmine T, Itoh H, Onohara T, Maehara Y (2010) The efficacy of oral beraprost sodium, a prostaglandin I₂ analogue, for treating intermittent claudication in patients with arteriosclerosis obliterans. *Int Angiol* 29(2 Suppl):49–54
- Peng L, Li J, Xu Y, Wang Y, Du H, Shao J, Liu Z (2016) The protective effect of beraprost sodium on diabetic nephropathy by inhibiting inflammation and p38 MAPK signaling pathway in high-fat diet/streptozotocin-induced diabetic rats. *Int J Endocrinol* 2016:1690474
- Takeshita K, Satoh M, Ii M, Silver M, Limbourg FP, Mukai Y, Rikitake Y, Radtke F, Gridley T, Losordo DW, Liao JK (2007) Critical role of endothelial Notch1 signaling in postnatal angiogenesis. *Circ Res* 100(1):70–78
- Kramann R, Tanaka M, Humphreys BD (2014) Fluorescence microangiography for quantitative assessment of peritubular capillary changes after AKI in mice. *J Am Soc Nephrol* 25(9):1924–1931
- Lameire N, Jager K, Van Biesen W, de Bacquer D, Vanholder R (2005) Chronic kidney disease: a European perspective. *Kidney Int Suppl* 68(99):S30–S38
- Zhang L, Wang F, Wang L, Wang W, Liu B, Liu J, Chen M, He Q, Liao Y, Yu X, Chen N, Zhang JE, Hu Z, Liu F, Hong D, Ma L, Liu H, Zhou X, Chen J, Pan L, Chen W, Wang W, Li X, Wang H (2012) Prevalence of chronic kidney disease in China: a cross-sectional survey. *Lancet* 379(9818):815–822
- Yokoyama C, Yabuki T, Shimonishi M, Wada M, Hatae T, Ohkawara S, Takeda J, Kinoshita T, Okabe M, Tanabe T (2002) Prostacyclin-deficient mice develop ischemic renal disorders, including nephrosclerosis and renal infarction. *Circulation* 106(18):2397–2403
- Sato N, Kaneko M, Tamura M, Kurumatani H (2010) The prostacyclin analog beraprost sodium ameliorates characteristics of metabolic syndrome in obese Zucker (fatty) rats. *Diabetes* 59(4):1092–1100
- Ballermann BJ, Obeidat M (2014) Tipping the balance from angiogenesis to fibrosis in CKD. *Kidney Int Suppl* (2011) 4(1):45–52
- Zafrani L, Ince C (2015) Microcirculation in acute and chronic kidney diseases. *Am J Kidney Dis* 66(6):1083–1094
- Watson EC, Grant ZL, Coultas L (2017) Endothelial cell apoptosis in angiogenesis and vessel regression. *Cell Mol Life Sci* 74(24):4387–4403
- Dimmeler S, Zeiher AM (2000) Endothelial cell apoptosis in angiogenesis and vessel regression. *Circ Res* 87(6):434–439
- O’Riordan E, Mendeleev N, Patschan S, Patschan D, Eskander J, Cohen-Gould L, Chander P, Goligorsky MS (2007) Chronic NOS inhibition actuates endothelial-mesenchymal transformation. *Am J Physiol Heart Circ Physiol* 292(1):H285–H294
- Otunctemur A, Ozbek E, Cakir SS, Polat EC, Dursun M, Cekmen M, Somay A, Ozbay N (2015) Pomegranate extract attenuates unilateral ureteral obstruction-induced renal damage by reducing oxidative stress. *Urol Ann* 7(2):166–171
- Rocha R, Funder JW (2002) The pathophysiology of aldosterone in the cardiovascular system. *Ann N Y Acad Sci* 970:89–100

30. Chen H, Sun F, Zhong X, Shao Y, Yoshimura A, Liu Y (2013) Eplerenone-mediated aldosterone blockade prevents renal fibrosis by reducing renal inflammation, interstitial cell proliferation and oxidative stress. *Kidney Blood Press Res* 37(6):557–566
31. Liang G, Song L, Chen Z, Qian Y, Xie J, Zhao L, Lin Q, Zhu G, Tan Y, Li X, Mohammadi M, Huang Z (2018) Fibroblast growth factor 1 ameliorates diabetic nephropathy by an anti-inflammatory mechanism. *Kidney Int* 93(1):95–109
32. Kolli VK, Abraham P, Rabi S (2008) Methotrexate-induced nitrosative stress may play a critical role in small intestinal damage in the rat. *Arch Toxicol* 82(10):763–770
33. Jiang L, Qiu W, Zhou Y, Wen P, Fang L, Cao H, Zen K, He W, Zhang C, Dai C, Yang J (2013) A microRNA-30e/mitochondrial uncoupling protein 2 axis mediates TGF-beta1-induced tubular epithelial cell extracellular matrix production and kidney fibrosis. *Kidney Int* 84(2):285–296
34. Chen JF, Wu QS, Xie YX, Si BL, Yang PP, Wang WY, Hua Q, He Q (2017) TRAP1 ameliorates renal tubulointerstitial fibrosis in mice with unilateral ureteral obstruction by protecting renal tubular epithelial cell mitochondria. *FASEB J* 31(10):4503–4514
35. Zhang S, Tan X, Chen Y, Zhang X (2017) Postconditioning protects renal fibrosis by attenuating oxidative stress-induced mitochondrial injury. *Nephrol Dial Transplant* 32(10):1628–1636
36. Inoue E, Ichiki T, Takeda K, Matsuura H, Hashimoto T, Ikeda J, Kamiharaguchi A, Sunagawa K (2012) Beraprost sodium, a stable prostacyclin analogue, improves insulin resistance in high-fat diet-induced obese mice. *J Endocrinol* 213(3):285–291
37. Yamada M, Sasaki R, Sato N, Suzuki M, Tamura M, Matsushita T, Kurumatani H (2002) Amelioration by beraprost sodium, a prostacyclin analogue, of established renal dysfunction in rat glomerulonephritis model. *Eur J Pharmacol* 449(1–2):167–176
38. Brenner BM, Lawler EV, Mackenzie HS (1996) The hyperfiltration theory: a paradigm shift in nephrology. *Kidney Int* 49(6):1774–1777
39. Zeisberg M, Neilson EG (2010) Mechanisms of tubulointerstitial fibrosis. *J Am Soc Nephrol* 21(11):1819–1834
40. Wei SY, Wang YX, Zhang QF, Zhao SL, Diao TT, Li JS, Qi WR, He YX, Guo XY, Zhang MZ, Chen JY, Wang XT, Wei QJ, Wang Y, Li B (2017) Multiple mechanisms are involved in salt-sensitive hypertension-induced renal injury and interstitial fibrosis. *Sci Rep* 7:45952
41. Sun D, Eirin A, Zhu XY, Zhang X, Crane JA, Woollard JR, Lerman A, Lerman LO (2015) Experimental coronary artery stenosis accelerates kidney damage in renovascular hypertensive swine. *Kidney Int* 87(4):719–727

Publisher's note Springer Nature remains neutral with regard to jurisdictional claims in published maps and institutional affiliations.